

HIGH RESOLUTION OBSERVATIONS OF CEN A: YELLOW AND RED SUPERGIANTS IN A REGION OF JET-INDUCED STAR FORMATION? *

MARKAKIS, K.^{1,2,5}, ECKART, A.^{1,2}, CASTRO, N.³, SÁNCHEZ-MONGE, Á.¹, LABADIE, L.¹, NISHIYAMA, S.⁴, BRITZEN, S.² AND ZENSUS, J. A.^{2,1}

(Received 27 Jun. 2017; Revised 09 Oct. 2017; Accepted 10 Oct. 2017)

¹I. Physikalisches Institut, Universität zu Köln, Zùlpicher Str. 77, 50937 Köln, Germany

²Max-Planck-Institut für Radioastronomie, Auf dem Hügel 69, 53121 Bonn, Germany

³University of Michigan, Department of Astronomy, 1085 S. University Avenue, Ann Arbor, MI 48109-1107, USA

⁴Miyagi University of Education, Sendai, Miyagi 980-0845, Japan

⁵markakis@ph1.uni-koeln.de

ABSTRACT

We present the analysis of near infrared (NIR), adaptive optics (AO) Subaru and archived HST imaging data of a region near the northern middle lobe (NML) of the Centaurus A (Cen A) jet, at a distance of ~ 15 kpc north-east (NE) from the center of NGC5128. Low-pass filtering of the NIR images reveals strong $> 3\sigma$ above the background mean $-$ signal at the expected position of the brightest star in the equivalent HST field. Statistical analysis of the NIR background noise suggests that the probability to observe $> 3\sigma$ signal at the same position, in three independent measurements due to stochastic background fluctuations alone is negligible ($\leq 10^{-7}\%$) and, therefore, that this signal should reflect the detection of the NIR counterparts of the brightest HST star. An extensive photometric analysis of this star yields $V - I$, visual-NIR, and NIR colors expected from a yellow supergiant (YSG) with an estimated age $\sim 10_{-3}^{+4}$ Myr. Furthermore, the second and third brighter HST stars are, likely, also supergiants in Cen A, with estimated ages $\sim 16_{-3}^{+6}$ Myr and $\sim 25_{-9}^{+15}$ Myr, respectively. The ages of these three supergiants are in good agreement with the ages of the young massive stars that were previously found in the vicinity and are thought to have formed during the later phases of the jet-HI cloud interaction that appears to drive the star formation (SF) in the region for the past ~ 100 Myr.

Keywords: techniques: image processing $-$ high angular resolution $-$ stars: supergiants $-$ galaxies: evolution $-$ galaxies: individual: NGC5128

1. INTRODUCTION

NGC5128 is located at a distance of ~ 3.8 Mpc (Rejkuba 2004) and is the host of the powerful extra-galactic radio source Centaurus A (Cen A). This peculiar giant elliptical galaxy is considered to be an example of a post-merging system, believed to have formed via the merging of a massive early-type and a smaller gas-rich galaxy (e.g. Malin et al. 1983; Israel 1998).

At ~ 15 kpc north-east (NE) from NGC5128's nucleus lies the northern middle lobe (NML) of Cen A. An HI cloud (Schiminovich et al. 1994; Oosterloo & Morganti 2005), CO molecular gas (Charmandaris et al. 2000), shells of old stars (Malin et al. 1983), filaments of ionized

gas (Morganti et al. 1991), young massive stars and OB associations (e.g. Blanco et al. 1975; Graham & Price 1981; Graham 1998; Fassett & Graham 2000; Mould et al. 2000; Rejkuba et al. 2001) have been previously identified near this position. All these are superimposed on a background sheet of older stars, typical of the halo of NGC5128 (Mould et al. 2000; Rejkuba et al. 2001).

Many authors (e.g. Graham 1998; Mould et al. 2000; Rejkuba et al. 2001) suggest that the presence of young massive stars in the region is the result of a recent jet-induced star forming episode, since both the gas clouds and the filaments of ionized gas appear to be associated with the young massive stars that lie along the NE edge of the HI cloud and into the jet's path (Fig. 1). Oosterloo & Morganti (2005) see anomalous velocities in the south-eastern (SE) tip of the HI cloud and they suggest that this is where the jet-HI cloud interaction

* Based on data collected at Subaru Telescope, which is operated by the National Astronomical Observatory of Japan.

takes place, while [Salomé et al. \(2016a\)](#) find that the gas in the outer filament is likely excited by energy provided by either AGN/shocks, star formation (SF), or a combination of these mechanisms.

The ages of the young massive stars of this region are estimated to be $\sim 10 - 15$ Myr, based on comparisons of their optical color-magnitude diagram (CMD) with both stellar evolutionary isochrones ([Fassett & Graham 2000](#); [Rejkuba et al. 2001](#)) and CMDs of young clusters in the Large Magellanic Cloud ([Mould et al. 2000](#)). [Rejkuba et al. \(2004\)](#) simulated the recent SF history (SFH) of the region by constructing synthetic CMDs for metallicities $Z = 0.004$ and $Z = 0.008$, assuming different SF durations and initial mass functions (IMF). A comparison of the synthetic CMDs and the blue main sequence (MS) luminosity functions with the ones observed by [Rejkuba et al. \(2001\)](#) revealed that the SF in the halo of NGC5128 is, likely, not an episodic event, but a continuous process for (at least) the last ~ 100 Myr, which has either ceased ~ 2.5 Myr ago, or is still ongoing. They also constrained the IMF slope $\alpha \sim 2 - 2.6$ and the SF rate $\sim 0.004 - 0.013 M_{\odot} yr^{-1}$. The simulations of [Rejkuba et al. \(2004\)](#) appear to be consistent with recent findings of [Salomé et al. \(2016b\)](#), who estimate the metallicity and the SF rate in the outer filament to be $\langle Z \rangle \sim 0.6 Z_{\odot} = 0.008$ and $\sim 0.004 M_{\odot} yr^{-1}$, respectively.

Within the suggested time-frames, many of these young massive stars are expected to have evolved past the MS. This makes the NE part of NGC5128 an excellent target for searching for extra-galactic NIR-excess sources, e.g. later-type–yellow (YSG) and red (RSG)–supergiants and asymptotic giant branch (AGB) stars, that should exist within the framework of a recent (jet-induced) SF. Attempting, therefore, to observe a denser-than-average region outside our Local Group (LG) in the NIR, using a state-of-the-art 8-m class telescope equipped with an adaptive optics (AO) system, is expected to reveal a wealth of information regarding the nature of its evolved massive stellar populations and, potentially, also of the history of the jet-HI cloud interaction itself.

This paper is organized as follows: In Sect. 2 we describe the data and photometric calibration; in Sect. 3 we describe the process of locating the Subaru field on archived HST images of the same region; in Sect. 4 we describe the near infrared (NIR) data processing and we attempt, both statistically and photometrically, to constrain the spectral types and luminosity classes of the three brighter stars in the HST field; and in Sect. 5 we discuss our results and the observational potential of using AO assisted observations in galaxies outside our LG.

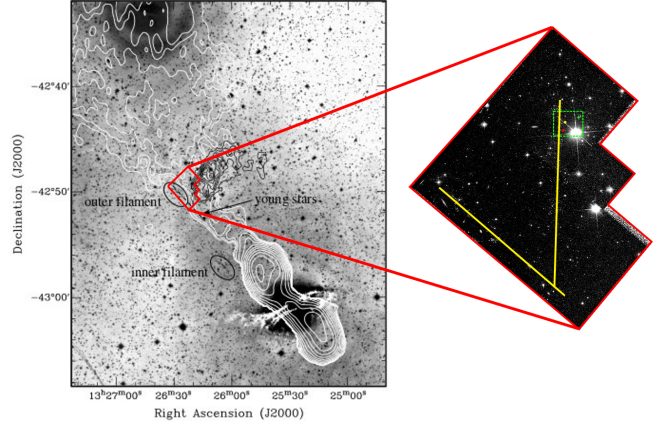


Figure 1. Left: Reproduction of Fig. 1 from [Oosterloo & Morganti \(2005\)](#). The centimeter radio jet (white contours), the HI cloud (black contours), and the filaments of ionized gas (black ellipses) are over-plotted on an optical image of NGC5128. The red outlined region indicates the approximate position and coverage of the HST field (right) studied by [Mould et al. \(2000\)](#). Right: The yellow lines on the HST $F555W$ image indicate the approximate positions of the young massive stars, while the green dashed rectangle indicates the Subaru field.

2. OBSERVATIONS AND DATA

2.1. Subaru data

The data-set used for studying the young stellar population along the jet of NGC5128 consists of AO assisted NIR data in the $J(10)$, $H(10)$, and $K_S(10)$ bands (number of images), taken on 2012 May 17, with the Subaru telescope at Mauna Kea, Hawaii, using the HiCIAO ([Suzuki et al. 2010](#)) instrument. The exposure time is $t_{exp}^{J,H,K_S} = 60$ sec for each individual frame in all bands. The AO188 AO system is used ([Hayano et al. 2010](#)). It is equipped with a 188-element wavefront curvature sensor with photon counting APD modules and a 188 element bimorph mirror, installed at the IR Nasmyth platform of the Subaru telescope. As a result, the angular resolution of the data is ~ 270 , ~ 210 , and ~ 170 mas for the J , H , and K_S bands, respectively. The 2048×2048 pixel² Hawaii-IIIRG HgCdTe detector provides a pixel scale of $0.010 \text{ arcsec pixel}^{-1}$ and a field of view (FoV) of $20 \times 20 \text{ arcsec}^2$. The studied field was chosen because of the presence of bright foreground natural guide stars, which is a prerequisite for the AO system to deliver the highest angular resolution possible.

No reduction package was available for HiCIAO, so a pipeline was developed from scratch in order to correct for the high frequency 32-strip artifact noise, introduced by the 32 readout channels of the detector. All images were dithered and have undergone the usual bad pixel correction, flat-fielding (dome-flat), sky-subtraction, alignment, and median stacking. Finally, we remove any large-scale patterns from our images by subtracting an image of the weighted average of the

mean row and column values, respectively. In all images north is up and east is left. The reduced ready-for-science $\sim 20 \times 18$ arcsec² J , H , and K_S images are shown in Fig. 2.

2.1.1. Subaru photometric calibration

The flux calibration of the Subaru data was performed using standard star observations in our data-set to derive appropriate zero points for the J , H , and K_S bands. Apparent magnitudes are then calculated using:

$$m_{Sub.}^i = Z.P.^i_{Sub.} - 2.5 \log\left(\frac{\text{Counts}_{Sub.}^i}{\text{Exp.Time}_{Sub.}^i}\right). \quad (1)$$

The two bright (AO guide) stars¹ in the bottom right corner of Fig. 2 can be used to test the quality of the photometric calibration against 2MASS photometry of the same sources. Due to the lower angular resolution of the 2MASS images, however, these sources appear as an unresolved point source² with $m_{2MASS\ G.S.}^{K_S} = 11.15 \pm 0.02$ mag, $m_{2MASS\ G.S.}^H = 11.30 \pm 0.04$ mag, and $m_{2MASS\ G.S.}^J = 11.51 \pm 0.03$ mag. The equivalent G.S. Subaru magnitudes are given by the sum of the fluxes of the SE (G.S.1) and the north-western (NW – G.S.2) guide stars, namely $m_{SUB.\ G.S.}^{K_S} = 11.17 \pm 0.14$ mag, $m_{SUB.\ G.S.}^H = 11.33 \pm 0.14$ mag, and $m_{SUB.\ G.S.}^J = 11.56 \pm 0.14$ mag. The very good agreement between 2MASS and Subaru magnitudes indicates that our calibration is fairly accurate, which allows us to use the two NIR guide stars as calibration reference sources for the rest of our magnitude estimations.

2.2. HST data

We also use archived HST $F555W$ and $F814W$ images of the same region, originally analyzed by Mould et al. (2000) (Fig. 3). We obtain $F555W$ and $F814W$ magnitudes for the stars in our interest, by performing aperture photometry. Transformations between the STMAG and the Johnson UBVRI photometric systems are subsequently performed according to the tables of the WFPC2 Photometry Cookbook/HST Data Handbook for WFPC2. Throughout this paper we adopt average $V - F555W = -0.01 \pm 0.06$ mag and $I - F814W = -1.30 \pm 0.24$ mag. We test the validity of the adopted transformations against the V band magnitudes and $V - I$ colors of the two brightest stars on the WF2 chip (see Table 1, Mould et al. 2000). Our measurements are within $\sim 5\%$ with respect to the published values, indicating that the chosen transformations are fairly accurate.

¹ Hereafter “guide stars”.

² Hereafter G.S.

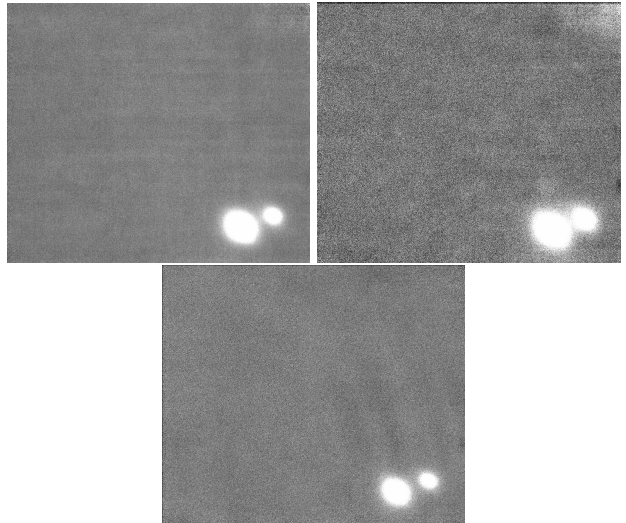


Figure 2. Subaru J (top left), H (top right) and K_S (bottom middle) bands, $\sim 20 \times 18$ arcsec² ready-for-science images.

3. LOCATING THE SUBARU FIELD

The Subaru field is located at ~ 15 kpc NE from the center of NGC5128, with central coordinates $\alpha_{2000} = 13^h 26^m 21^s.127$ and $\delta_{2000} = -42^\circ 49' 09''.02$. In order to precisely locate it on the HST images (Fig. 3), we use the two guide stars and the cardinal directions as reference points.

The projected separations and position angles (PA) of the guide stars are 2.19 ± 0.14 and 2.25 ± 0.01 arcsec and 19.3 ± 1.0 and 19.0 ± 0.1 degrees on the HST and Subaru images³, respectively. These indicate that the guide stars are either an apparent projected, or a long period physical and not a close physical binary system. The insignificant change in their separation and PA between the epochs of the HST and the Subaru data (i.e. ~ 15 yrs) could be the result of either a “lucky” snapshot of a close physical binary in the same orbital configuration as on the HST images, or the combination of the different (yet negligible) proper motions of the two projected members. The latter seems more likely in a, time-wise, random observation.

Moreover, the total (i.e. over 15 yrs) G.S. proper motion of 24.2 ± 14.3 mas in RA and -34.5 ± 12.0 mas in Dec (UCAC4 catalog, Zacharias et al. 2013) can, in principal, account for the small changes in the separation and PA of the guide stars. Most importantly though, the negligible G.S. proper motion indicates that the HST

³ The centers of both Subaru guide stars and of the fainter (NW) HST guide star are estimated by Gaussian fitting on the point-spread-function (PSF). For the brighter (SE) HST guide star, however, we use the central pixel of the saturated peak of the PSF as an acceptable center estimation, but with a significantly larger uncertainty.

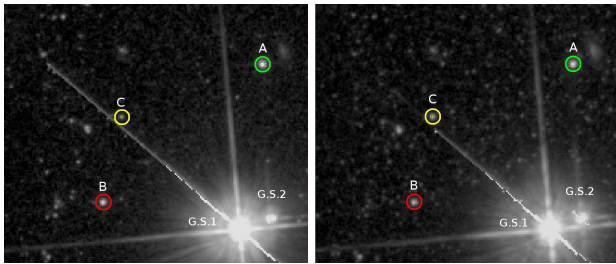


Figure 3. HST $F555W$ (left) and $F814W$ (right) images. This is the equivalent to the Subaru J , H , and K_S field ($\sim 20 \times 18$ arcsec²). The colored circles mark the positions of the three brighter stars on the $F814W$ HST field. The A HST star is the brightest, the B is the second brighter, and the C is the third brighter.

field stars⁴ are expected to be found at, roughly, the same—relative to the guide stars—positions on the Subaru J , H , and K_S images as well.

4. DATA PROCESSING

Initially, there is no obvious signal on the Subaru images (Fig. 2) that can be directly correlated with the HST field stars (Fig. 3). We apply a low-pass filter with a 10-pixel Gaussian kernel on the NIR data, in order to increase the signal-to-noise-ratio (SNR) and highlight any signal that might be embedded into the noise. A JHK_S composite image is also constructed from the low-pass filtered NIR images (using equal weighting for each band), to achieve a further increase of the SNR by a factor of $\sim \sqrt{3}$ (Fig. 4).

All the low-pass filtered images of Fig. 4 show *strong signal* at the expected position of the brightest HST field star (A HST star – the star in the green circle in Fig. 3). The peak flux of this signal is $> 3\sigma$ above the background mean, while this is the only position where a signal with these characteristics is consistently present in all NIR bands⁵ (Fig. 5). Since the field stars are expected to be found at the same positions on both the Subaru and the HST images, can the observed $> 3\sigma$ signal come from the NIR counterparts of the A HST star and, if yes, can we constrain its nature? Answering this requires both a statistical and a photometric analysis.

⁴ The term “field stars” refers to the faint background stars seen on the HST images (Fig. 1 and 3), which are thought to be part of the young blue stars along the Cen A jet.

⁵ For the H band this refers to the northern peak. The southern peak is not present in any other NIR band, which suggests that it could have originated from a low/moderate (e.g. a $\sim +0.5 - 1\sigma$) random noise fluctuation superimposed on the $> 3\sigma$ signal, mimicking a secondary peak feature. Such a small random fluctuation, however, could occur with a rather significant probability of $\sim 15 - 30\%$. Therefore, we do not consider it as a true signal for the rest of this work. We refer the reader to Sect. 4.1 for a more extended discussion on the background noise of an astronomical image.

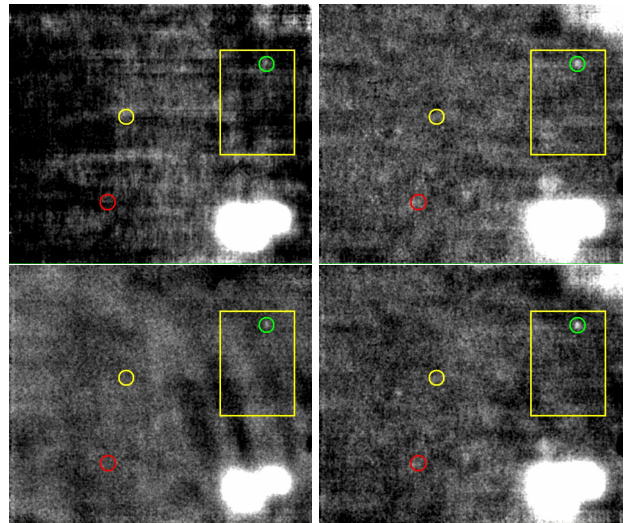


Figure 4. Subaru J (top left), H (top right), K_S (bottom left), and the JHK_S composite (bottom right) images, low-pass filtered with a 10-pixel Gaussian kernel. The three colored circles mark the expected positions of the three brighter stars on the HST $F814W$ field, while the $\sim 5 \times 7$ arcsec² statistics region is outlined by the yellow box.

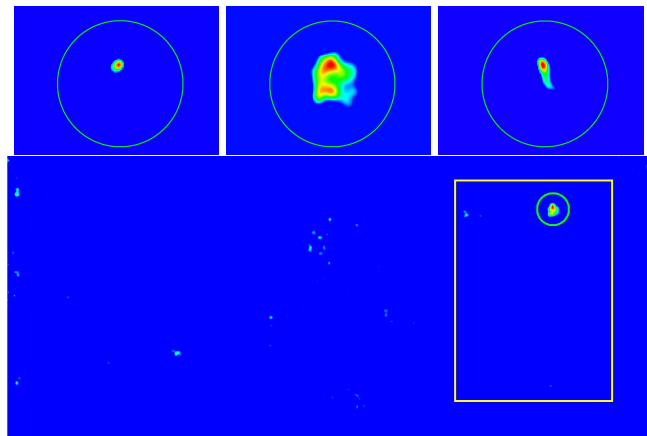


Figure 5. Top: The $> 3\sigma$ NIR signal at the expected position of the A HST star (zoomed-in region) in the Subaru J (left), H (middle), and K_S (right) bands, respectively. Bottom: A $\sim 20 \times 9$ arcsec² region of the Subaru JHK_S composite with the statistics region outlined by the yellow box ($\sim 5 \times 7$ arcsec²). All images are low-pass filtered with a 10-pixel Gaussian Kernel and clipped at 3σ above the background mean (blue background).

4.1. Statistical analysis of the NIR signal

Approaching the above question statistically means that we have to formulate it in a more mathematical way: What is the probability to observe $> 3\sigma$ signal at the same position in three independent experiments, if it results from stochastic background noise fluctuations alone?

Generally, the values of the background noise of an astronomical image follow the Poisson distribution, which for large statistical samples should approach the

Gaussian distribution. Given a Gaussian distribution, the probability to randomly draw (observe) a variable (a flux value) F_i that satisfies the condition

$$\bar{F}_{bg} - 3\sigma \geq F_i \text{ and } F_i \geq \bar{F}_{bg} + 3\sigma ,$$

where \bar{F}_{bg} is the mean (mean flux) of the distribution, from a single experiment (observation) is $\leq 0.27\%$.

We perform our statistical analysis in a sub-region of $\sim 5 \times 7$ arcsec² (yellow box in Figs. 4 and 5, $N \sim 3.5 \times 10^3$ pixels), including the position of the A HST star. Given the large statistical sample, the background noise distribution is expected to be very close to normal. Our measurements within this sampling area support this view, since the mean and the median converge, implying a) that the distribution is not heavy tailed and, more importantly, b) that the chosen statistical sample represents the global statistics well, at least, in terms of statistical power.

Therefore, if we randomly select a pixel inside our sampling area from one observation, the probability to observe a value $\geq 3\sigma$ above the background mean is $\leq 0.135\%$ or $P(A) \leq 0.00135^6$. Considering also that the $> 3\sigma$ signal at the position of the A HST star is the only consistently present signal in all our NIR images (i.e. three independent experiments), then the probability that it results from random background noise fluctuations should be $[P(A)]^3 \leq 2.5 \times 10^{-9}$ or $\leq 2.5 \times 10^{-7}\%$. Since this is negligible, we can safely consider that the presence of an underlying point source, which systematically “drives” the flux within the green circle above the $+3\sigma$ limit in repeated observations, is the origin of the observed $> 3\sigma$ NIR signal of Fig. 5.

Are, however, the photometric properties of the $> 3\sigma$ NIR detections consistent with the visual photometric properties of the A HST star?

4.2. Photometric calibration of the NIR detections

The V and I magnitudes of the A HST star are measured with aperture photometry on the $F555W$ and $F814W$ HST images (Sect. 2.2). They are $m_{HST,A}^V = 20.23 \pm 0.12$ and $m_{HST,A}^I = 19.39 \pm 0.26$ mag, respectively.

On the contrary, due to the low SNR of the Subaru data, aperture photometry is not an option for estimating the NIR magnitudes of the $> 3\sigma$ detections. Alternatively, their $J, H,$ and K_S magnitudes are estimated by taking the ratio of the sum of the peak

fluxes of G.S.1 and G.S.2 to the peak fluxes of the $> 3\sigma$ NIR detections⁷, using

$$m_{>3\sigma}^{J,H,K_S} = m_{G.S.}^{J,H,K_S} + 2.5 \times \log X \quad (2)$$

$$\text{with, } X = \left(\frac{F_{G.S.1}^{J,H,K_S} + F_{G.S.2}^{J,H,K_S}}{F_{>3\sigma}^{J,H,K_S}} \right) ,$$

where, $F_{G.S.i}^{J,H,K_S}$ is the peak flux of each guide star, $F_{>3\sigma}^{J,H,K_S}$ is the peak flux of each $> 3\sigma$ detection, and $m_{G.S.}^{J,H,K_S}$ is the Subaru $J/H/K_S$ magnitude of the G.S. that we derived in Sect. 2.1.1.

This yields $m_{>3\sigma}^{K_S} = 18.15 \pm 0.37$, $m_{>3\sigma}^H = 18.51 \pm 0.36$, and $m_{>3\sigma}^J = 18.96 \pm 0.36$ magnitudes for the $> 3\sigma$ detections in each NIR band. The uncertainties are calculated according to the relation:

$$\delta m_{>3\sigma}^{J,H,K_S} = \left((\delta m_{G.S.}^{J,H,K_S})^2 + 0.43^2 \times 2.5^2 \times \left(\frac{\delta X}{X} \right)^2 \right)^{1/2} \quad (3)$$

$$\text{with, } \left(\frac{\delta X}{X} \right)^2 = \frac{(\delta F_{G.S.1}^{J,H,K_S})^2 + (\delta F_{G.S.2}^{J,H,K_S})^2}{(F_{G.S.1}^{J,H,K_S} + F_{G.S.2}^{J,H,K_S})^2} + \left(\frac{\delta F_{>3\sigma}^{J,H,K_S}}{F_{>3\sigma}^{J,H,K_S}} \right)^2$$

$$\text{and } (\delta m_{G.S.}^{J,H,K_S})^2 = (\delta m_{G.S.1}^{J,H,K_S})^2 + (\delta m_{G.S.2}^{J,H,K_S})^2$$

where we assume a 10% uncertainty in the measurement of $F_{G.S.i}^{J,H,K_S}$ and a 30% uncertainty in the measurement of the, more uncertain, $F_{>3\sigma}^{J,H,K_S}$.

Having magnitude estimations, we can attempt to constrain the $V - I$, visual-NIR⁸, and NIR⁹ colors of the $> 3\sigma$ NIR detections/A HST star and, therefore, its spectral type and luminosity class.

4.3. An extra-galactic supergiant or a galactic dwarf?

There are two possibilities for the nature of the A HST star. It can be either a distant supergiant belonging to the recently formed stars along the Cen A jet or a faint MS dwarf belonging to our own Milky Way galaxy. Following the intrinsic colors of supergiants and MS stars given by [Ducati et al. \(2001\)](#) (Table 1), the $V - I = 0.84 \pm 0.28$ color of the A HST star is consistent with either an $F8 - G3$ supergiant, or an $F5 - K1$ MS dwarf.

The primary criterion used to assign a spectral type to the A HST star is the $V - I$ color, because of its smaller uncertainty. As a secondary criterion we use the visual-NIR colors, in order to check for inconsistencies

⁶ $P(A) \leq 0.0027$ is the probability to observe values outside the $\bar{F}_{bg} \pm 3\sigma$ limits. Half of this should account for the probability to observe values that exceed only the upper limit of $+3\sigma$. Therefore, a $P(A) \leq 0.00135$ is adopted as a realistic occurrence probability of a stochastic $\geq 3\sigma$ observation in a single experiment.

⁷ Point sources of different brightness observed simultaneously with the same telescope are convolved with the same PSF as long as their separation is smaller than ~ 30 arcsec (i.e. isoplanatic angle). Consequently, the ratio of the fluxes at any point across their PSFs and the ratio of their integrated fluxes will (ideally) be approximately equal and, therefore, any of these measurements should be representative of their true brightness difference.

⁸ i.e. $V - J$, $V - H$, and $V - K_S$.

⁹ i.e. $J - H$, $H - K_S$, and $J - K_S$.

Table 1. NIR and Visual-NIR colors.

Colors	$V - I$	$V - J$	$V - H$	$V - K_S$	$J - H^a$	$H - K_S^a$	$J - K_S^a$
A HST Star	0.84	1.27	1.72	2.08	0.45	0.36	0.81
Uncertainties	(± 0.28)	(± 0.38)	(± 0.38)	(± 0.39)	(± 0.51)	(± 0.52)	(± 0.52)
Spectral Type	Intrinsic colors of Supergiants (Ducati et al. 2001)						
A5	0.180	0.200	0.290	0.350	0.090	0.060	0.150
F0	0.310	0.360	0.510	0.600	0.150	0.090	0.240
F2	0.370	0.440	0.620	0.730	0.180	0.110	0.290
F5	0.470	0.570	0.790	0.910	0.220	0.120	0.340
F8	0.700	0.870	1.170	1.340	0.300	0.170	0.470
G0	0.900	1.140	1.520	1.710	0.380	0.190	0.570
G2	1.060	1.350	1.800	1.990	0.450	0.190	0.640
G3	1.120	1.430	1.900	2.090	0.470	0.190	0.660
G3.5	1.160	1.470	1.950	2.150	0.480	0.200	0.680
G4	1.190	1.520	2.010	2.200	0.490	0.190	0.680
G5	1.260	1.610	2.130	2.320	0.520	0.190	0.710
G8	1.430	1.830	2.410	2.590	0.580	0.180	0.760
K0	1.590	2.010	2.640	2.800	0.630	0.160	0.790
K1	1.680	2.110	2.760	2.910	0.650	0.150	0.800
K2	1.760	2.200	2.870	3.010	0.670	0.140	0.810
K3	1.960	2.410	3.140	3.250	0.730	0.110	0.840
K3.5	2.040	2.500	3.250	3.340	0.750	0.090	0.840
K4	2.130	2.590	3.370	3.440	0.780	0.070	0.850
K5	2.270	2.740	3.550	3.590	0.810	0.040	0.850
Spectral Type	Intrinsic colors of MS Stars (Ducati et al. 2001)						
A9	0.310	0.310	0.490	0.440	0.180	-0.050	0.130
F0	0.360	0.370	0.570	0.520	0.200	-0.050	0.150
F1	0.400	0.430	0.640	0.580	0.210	-0.060	0.150
F2	0.450	0.480	0.710	0.660	0.230	-0.050	0.180
F5	0.570	0.670	0.930	0.890	0.260	-0.040	0.220
F8	0.640	0.790	1.060	1.030	0.270	-0.030	0.240
G0	0.700	0.870	1.150	1.140	0.280	-0.010	0.270
G2	0.750	0.970	1.250	1.260	0.280	0.010	0.290
G3	0.760	0.980	1.270	1.280	0.290	0.010	0.300
G5	0.780	1.020	1.310	1.320	0.290	0.010	0.300
G8	0.850	1.140	1.440	1.470	0.300	0.030	0.330
K0	0.970	1.340	1.670	1.740	0.330	0.070	0.400
K1	1.050	1.460	1.800	1.890	0.340	0.090	0.430
K2	1.140	1.600	1.940	2.060	0.340	0.120	0.460
K3	1.250	1.730	2.090	2.230	0.360	0.140	0.500
K4	1.340	1.840	2.220	2.380	0.380	0.160	0.540
K5	1.540	2.040	2.460	2.660	0.420	0.200	0.620
K7	1.860	2.300	2.780	3.010	0.480	0.230	0.710
M0	2.150	2.490	3.040	3.290	0.550	0.250	0.800
M1	2.360	2.610	3.220	3.470	0.610	0.250	0.860
M2	2.620	2.740	3.420	3.670	0.680	0.250	0.930
M3	2.840	2.840	3.580	3.830	0.740	0.250	0.990
M4	3.070	2.930	3.740	3.980	0.810	0.240	1.050

NOTE—Top: $V - I$, Visual-NIR, and NIR colors for the A HST star/Subaru NIR detections with their corresponding uncertainties. Middle/Bottom: The intrinsic colors of supergiants and main-sequence stars from Ducati et al. (2001). The $V - I$, Visual-NIR (red), and NIR (blue) color ranges of the A HST star/Subaru NIR detections are marked in the middle and bottom tables, indicating a potential spectral type range for each luminosity class.

^aThe $J - H$, $H - K_S$, and $J - K_S$ indices for the middle and bottom tables are calculated from the $-(V - J) + (V - H)$, $-(V - H) + (V - K_S)$, and $-(V - J) + (V - K_S)$, respectively.

in their overlap with the $V - I$. Finally (and for completeness), we also examine the overlap of the NIR with the other colors for each luminosity class. The results are presented in Table 1.

The $V - I$ and visual-NIR colors of the A HST star

suggest limited spectral type ranges, which, generally, agree for both luminosity classes, although in the case of supergiants the color overlap is nearly perfect. On the other hand, the NIR colors suggest much larger spectral type ranges for both luminosity classes, but despite they clearly overlap with the $V - I$ and visual-NIR colors, they cannot be individually used to draw useful conclusions.

We note that we do not correct for reddening as its exact value on the lines-of-sight towards our objects cannot be precisely known. According to the IRSA on-line dust extinction tool¹⁰, however, the extinction on large-scale arcmin-scales towards NGC5128 should not be significant. Its effect on the colors of the A HST star would be a reduction of the $V - I$ by ~ 0.12 mag, of the visual-NIR by $\sim 0.20 - 0.24$ mag, and of the NIR colors by $\sim 0.02 - 0.04$ mag. These extinction corrections are in excellent agreement with recent higher resolution-results from Salomé et al. (2016a) for regions near our field. Accounting for these would shift our classifications towards ~ 1 spectral type earlier in Table 1, which will not, qualitatively at least, affect our interpretation.¹¹

So, is there a way to further distinguish between the extra-galactic supergiant and the galactic dwarf scenarios?

4.3.1. Supergiant

If the A HST star is an extra-galactic supergiant, then the remaining steps are relatively straightforward. Adopting a distance modulus for NGC5128 of $\mu = 27.92 \pm 0.19$ mag (Rejkuba 2004), its absolute magnitude $M_{HST,A}^V = -7.69 \pm 0.22$ mag combined with its $V - I$ color range place the A HST star in the region of the Hertzsprung-Russell (HR) diagram occupied by YSGs (e.g a G1). In order to estimate its age, we use isochrones for rotating and non-rotating stars with $Z = Z_\odot$ from Ekström et al. (2012) and isochrones for non-rotating stars with solar and sub-solar (i.e. $Z \sim 0.6Z_\odot$, Rejkuba et al. 2001; Salomé et al. 2016b) metallicities from Bertelli et al. (2009). The best fitting isochrones indicate an age¹² of $\sim 10_{-3}^{+4}$ Myr for the A HST star. An example of the isochrones used is shown in the visual-NIR CMD of figure 6.

Finding young supergiants in this part of Cen A, however, should not be a surprise. Earlier HST (Mould et al. 2000) and VLT observations (Rejkuba et al. 2001) confirmed the presence of young massive stars in the region,

¹⁰ <http://irsa.ipac.caltech.edu/applications/DUST/>

¹¹ Visually, this shift would place our stars near the left tip of their horizontal error-bars in the visual-NIR CMD of figure 6.

¹² The age is calculated as the median age of the within-the-photometric-uncertainties isochrones from all the models we used.

likely to have formed during the most recent phases of the jet-HI cloud interaction that powers the SF of the region over the last ~ 100 Myr (Rejkuba et al. 2004). In such a framework young, later-type supergiants are naturally expected in the vicinity, since the most massive ($\gtrsim 15 - 20 M_{\odot}$) of the later ($\lesssim 10 - 15$ Myr) generations of blue MS stars are expected to have evolved past the MS.

4.3.2. Dwarf

If the A HST star is a foreground MS dwarf, then we need to constrain its distance in order to get an estimate on its location within our Galaxy.

According to the suggested $V - I$ range (lower Table 1), its spectral type should be between $F5$ and $K1$. Assuming an intermediate spectral type to this range (e.g. $G3$), the expected absolute magnitude of the A HST star should be $M_{G3}^V \sim 5.10_{-1.40}^{+1.10}$ mag. From this and its apparent magnitude follows its distance modulus $\mu \sim 15.13_{-1.10}^{+1.40}$ mag and, therefore, its luminosity distance $D_L^{G3 \text{ dwarf}} \sim 10.62_{-4.22}^{+9.61}$ kpc. Accounting also for its galactic latitude of 19.6° , it should be located at a vertical to the galactic plane distance of $D_{\perp}^{G3 \text{ dwarf}} \sim 3.56_{-1.41}^{+3.23}$ kpc. The latter suggests that if the A HST star is a galactic source, then it should be located inside the (low density) stellar halo of the Milky Way (e.g. Voigt 1988; Norris 1997).

Adopting a galactic stellar halo density profile from Deason et al. (2011) and integrating over the solid angle defined by the HiCIAO FoV along the line-of-sight towards Cen A, we can estimate the theoretical fraction of galactic halo stellar mass that we expect to probe with our field. This corresponds to a total stellar mass of $M_{Fov}^{Total} \sim 0.39_{-0.23}^{+0.39} M_{\odot}^{13}$ and it could represent a $K0 - M8$ MS dwarf, assuming that the total probed stellar mass present in our field is in the form of one halo star. This mass range, however, overlaps only marginally with the potential mass range of the A HST star, namely, $\sim 0.7 - 1.3 M_{\odot}^{14}$. Considering also a) that the IMF peaks at $\sim 0.18 - 0.25 M_{\odot}$ and traces the present day mass function (PDFM) for low mass stars relatively accurately (e.g. Bochanski et al. 2010) and b) that the color overlap is not as consistent as in the case of supergiants, makes the galactic dwarf scenario significantly less likely for the A HST star, although it cannot be conclusively excluded.

¹³ The upper and lower limits reflect the different mass-to-light ratios assumed for the stellar halo of the Milky Way by Deason et al. (2011), i.e. $\sim 1 - 5$.

¹⁴ Corresponding to spectral types $\sim F5 - K1$.

4.4. What about the second and the third brighter HST stars?

The analysis, so far, suggests that the $> 3\sigma$ NIR signal that we detect comes from the NIR counterparts of the brighter star in the HST field, which, likely, is an extra-galactic YSG located in a region of recent jet-induced SF in the halo of NGC5128. We do not detect, however, neither the second (B HST star) nor the third (C HST star) brighter HST stars (Fig. 3) in the NIR.

Similarly to Sect. 4.3, we attempt to constrain the spectral types of the B and C HST stars (using only their $V - I$ colors) for both luminosity classes and estimate the corresponding quantities for the extra-galactic supergiant and foreground dwarf scenarios. The results are summarized in Table 2.

If these are extra-galactic stars, then their HST V band photometry (upper Table 2) and the distance modulus of NGC5128 suggest absolute visual magnitudes that place them in the supergiant region of the HR diagram. According to these and their $V - I$ color ranges, the B HST star is a YSG (i.e. an $F8$), while the C HST star is an RSG (i.e. a $K3/3.5$). Similarly to Sect. 4.3.1, we use various isochrones in order to estimate the ages of the B and C HST stars, namely, $\sim 16_{-3}^{+6}$ Myr and $\sim 25_{-9}^{+15}$ Myr, respectively.

In the supergiant scenario, therefore, both of these stars appear to be older than the A HST star. Despite the uncertainties in our age estimations this could be viewed as an additional indication that the recent SF in the halo of NGC5128 is not the result of a single episodic SF event, but rather of a continuous process (Rejkuba et al. 2004).

If these stars are foreground MS dwarfs (lower Table 2), then their expected vertical to the galactic plane distances would place them inside the stellar halo of the Milky Way. Similarly to Sect. 4.3.2, their spectral type ranges suggest potential masses of $\sim 0.8 - 1.5 M_{\odot}$ for the B and $\sim 0.5 M_{\odot}$ for the C HST stars. Evidently, the total expected stellar halo mass probed by the HiCIAO FoV overlaps with the expected mass of the C HST star, but not with that of the B HST star. This makes the galactic dwarf scenario potentially plausible only for the C HST star, leaving the B HST star as a good candidate supergiant in Cen A.

As noted earlier (Sect. 4.3.2), however, the C HST star can be considered as a foreground star under the assumption that all the expected halo stellar mass within our field is in the form of one halo star. Under the more conservative assumption that the probed halo stellar mass is in the form of the sum of a few lower mass stars near the peak of the IMF/PDMF (i.e. $\sim M5 - M8$), we consider as reasonable to treat the C HST star as a supergiant in Cen A for the rest of this work, since ac-

Table 2. Parameters for the B and C HST stars.

Extra-galactic Supergiant								
HST Star	$V - I$	S.T.R.	I.S.T. ^a	m_V	M_V	Exp. m_{K_S}	Exp. m_H	Exp. m_J
units	mag	-	-	mag	mag	mag	mag	mag
uncert.	± 0.28	-	-	± 0.12	± 0.22	-	-	-
B (red)	0.68	$F5 - G0$	$F8$	21.24	-6.68	$19.90^{+0.43}_{-0.37}$	$20.07^{+0.38}_{-0.35}$	$20.37^{+0.30}_{-0.27}$
C (yellow)	1.97	$K2 - K4$	$K3/3.5$	23.20	-4.72	$19.91^{+0.28}_{-0.15}$	$20.01^{+0.32}_{-0.18}$	$20.75^{+0.25}_{-0.14}$
Galactic Dwarf								
HST Star	$V - I$	S.T.R.	I.S.T. ^a	m_V	μ	Lum. Dist.	Vert. Dist.	
units	mag	-	-	mag	mag	kpc	kpc	
uncert.	± 0.28	-	-	± 0.12	-	-	-	
B (red)	0.68	$F1 - G8$	$G0$	21.24	$16.54^{+1.50}_{-0.90}$	$20.32^{+20.23}_{-6.89}$	$6.82^{+6.78}_{-2.31}$	
C (yellow)	1.97	$K7 - M0$	$K7/M0$	23.20	$14.80^{+0.30}_{-0.30}$	$9.12^{+1.35}_{-1.18}$	$3.06^{+0.45}_{-0.40}$	

NOTE—The first five columns are common in both tables. These indicate 1) the HST star identification corresponding to the letters/colored apertures of Fig. 3, 2) the $V - I$ color, 3) the spectral type range (S.T.R.) constrained through the suggested $V - I$ color on Table 1, 4) the intermediate spectral type (I.S.T.), and 5) the apparent V band magnitude. Top table: For the extra-galactic supergiant scenario, column 6) shows the absolute V band magnitude assuming a distance modulus of $\mu = 27.92 \pm 0.19$ mag for NGC5128, while columns 7), 8), and 9) show the expected K_S , H , and J band apparent magnitudes, respectively, assuming $V - K_S$, $V - H$, and $V - J$ colors from Table 1, for the chosen I.S.T. Bottom table: For the galactic dwarf scenario, column 6) shows the estimated distance modulus for the chosen I.S.T., column 7) shows the estimated luminosity distance, and column 8) shows the estimated vertical to the galactic plane (luminosity) distance, using a galactic latitude of $\sim 19.6^\circ$.

^aThe I.S.T. is chosen to be the middle spectral type of the corresponding S.T.R., or the average of the middle spectral types in the case of an even S.T.R. If the S.T.R. consists only of two spectral types, then the I.S.T. is their average. The uncertainties in the columns 7), 8), and 9) of extra-galactic supergiants and 6), 7), and 8) of galactic dwarfs cover the entire corresponding S.T.Rs.

counting for either two, or three candidate supergiants will not alter our conclusions.

This view is also supported by the work of Rejkuba et al. (2001). They corrected their 6.8×6.8 arcmin FORS1 data of the region for foreground contamination using a Besancon group stellar population synthesis model (Robin & Creze 1986; Robin et al. 1996) of the Milky Way and they estimate the number of foreground stars to be $\sim 340^{15}$. Taking into account that the foreground stars are distributed homogeneously across their FoV (see their Fig. 15) and scaling the estimated number with the area, we expect $\lesssim 0.8$ foreground stars in our 20×20 arcsec FoV, which suggests that all three HST stars are later-type supergiants in Cen A, in very good agreement with our earlier estimations.

5. DISCUSSION

We have extensively studied high resolution Subaru J , H , and K_S and archived HST $F555W$ and $F814W$ imaging data of a region along the Cen A's jet path, in which jet-induced SF is thought to be taking place.

We show that the NIR signal that we detect is statis-

tically significant and that it originates from the position of the A HST star, the brighter field point source detected on the HST imaging data. Its characteristics are constrained using its $V - I$, visual-NIR, and NIR color indices, which suggest that, most likely, this star is a YSG located in Cen A. Similarly, but based only on their HST photometry (i.e. on the $V - I$ color), the extra-galactic supergiant scenario is promoted also for the B (YSG) and C (RSG) HST stars.

5.1. Evolved massive stars in Cen A

The presence of later-type supergiants should be expected in this part of Cen A. Earlier studies (e.g. Fassett & Graham 2000; Mould et al. 2000; Rejkuba et al. 2001) have found young massive stars in this region, likely to have formed during the later ($\lesssim 10 - 15$ Myr) phases of the jet-HI cloud interaction that is thought to drive the local SF over the last ~ 100 Myr (Rejkuba et al. 2004). Our age estimates for the A, B, and C HST stars ($\sim 10_{-3}^{+4}$, $\sim 16_{-3}^{+6}$, and $\sim 25_{-9}^{+15}$ Myr, respectively) appear to be consistent with a continuous SF process, although their uncertainties do not allow us to conclusively confirm it. Nonetheless, supergiants of different ages would naturally fit in such a framework, since a ~ 100 Myr period of jet-HI gas interaction is expected to have created multiple generations of blue massive stars,

¹⁵ For a photometric depth of $V = 25$ mag. This number should be, at most, an upper limit for our case, since the HST data used here have a photometric depth of ~ 24 mag (Mould et al. 2000).

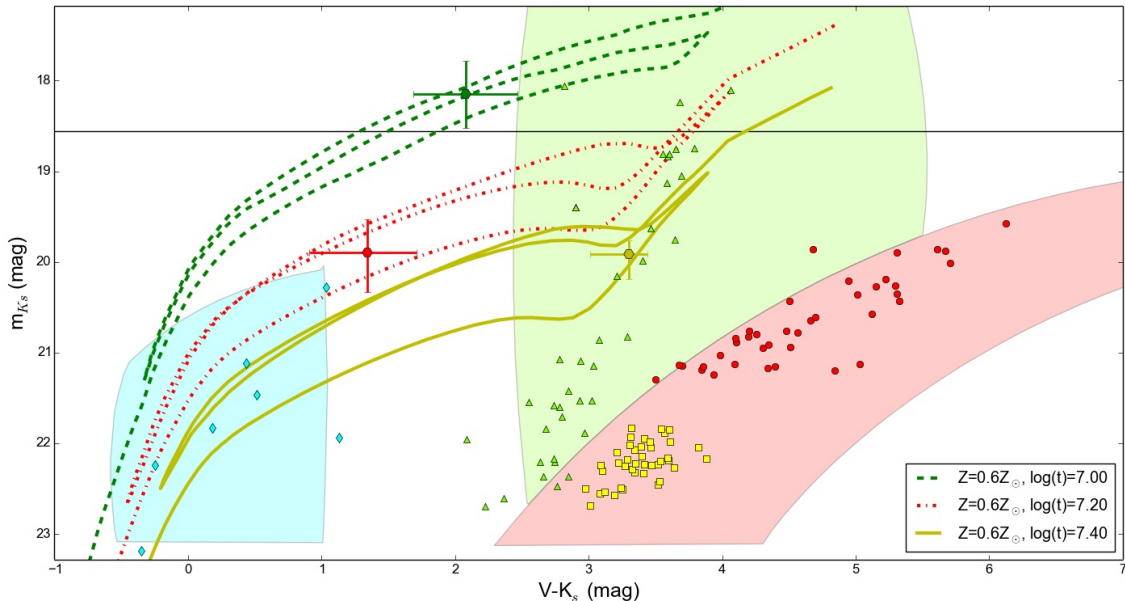


Figure 6. Visual-NIR CMD of Fig. 3 from Gullieuszik et al. (2008). Plotted are the BSGs (diamond symbols), RSGs (triangles), RGB (squares), and AGB (filled circles) stars of UKS 2323-326. The red, green, and blue shaded areas indicate the respective stellar sequences of the NE part of NGC5128’s halo, estimated from Fig. 12 of Rejkuba et al. (2001). The green, red, and yellow points with the error bars indicate the positions of the A, B, and C HST stars, respectively, on the CMD and their corresponding uncertainties. The dashed (green), the dashed-dotted (red), and the solid (yellow) lines are the isochrones from Bertelli et al. (2009) for the median ages of the A, B, and C HST stars, respectively. Finally, the black solid line indicates the Subaru K_s limiting magnitude.

each one evolving from the MS to the supergiant phase at a different (mainly mass-dependent) pace.

Future, deep, spectro-photometric, optical/NIR AO observations of the entire region are expected to put a much better constraint on the ages of these evolved massive stars, which, along with their spatial distribution, would help us “reverse engineer” the most recent history of the jet-HI cloud interaction in Cen A, by investigating for example whether the jet is precessing, or not (e.g. Rejkuba et al. 2002). Since this is our closest known paradigm of such an interaction, understanding the properties of the evolved massive stellar populations of the region is essential for a deeper understanding of the underlying physics of positive AGN feedback.

Finally, finding candidate YSGs is also important for developing the stellar evolutionary theory, since the post MS evolution of massive stars is still uncertain (e.g. Langer 2012). YSGs are located in the instability strip ($T_{eff} \sim 5000 - 6000$ K) at the upper-part of the HR diagram in the so-called “HR gap” (e.g. Castro et al. 2014) and they can be either evolving from the MS to later spectral types, or from the RSG phase to earlier spectral types (e.g. Gordon et al. 2016). Both of these transitions are predicted to occur very quickly during the post MS phase, which can explain the small number of stars detected in the HR gap (e.g. Langer 2012). In this sense, each candidate YSG detected is important, since it can provide further empirical constraints to the

stellar evolutionary theory.

5.2. Resolving extra-galactic stars beyond our LG

Our attempt to resolve individual stars in galaxies outside our LG, with 8-m class telescopes observations, is not the first. Various authors (e.g. Bresolin et al. 2001, 2002; Castro et al. 2008; Ohya & Hota 2013) have conducted spectroscopic studies of isolated O and B stars in several nearby galaxies, while Rejkuba et al. (2001) photometrically studied two fields in the stellar halo of NGC5128 (including our field) using FORS1/ISAAC VLT observations. These studies, however, do not use AO assisted observations.

The only AO assisted study of extra-galactic stellar populations to our knowledge was performed by Gullieuszik et al. (2008), using MAD/VLT observations. In their study of the central region of the dwarf irregular galaxy UKS 2323-326, they resolved blue supergiants (BSGs), RSGs, red giant branch (RGB), and AGB stars down to ~ 22 mag in the K_s band. This study is the most relevant to ours, since we both used AO assisted ground-based observations in order to resolve denser-than-average extra-galactic fields.

A direct comparison between the stellar populations of NGC5128 and UKS 2323-326 is shown in Fig. 6. In this plot we show the CMD of Fig. 3 from Gullieuszik et al. (2008), with our A, B, and C HST stars over-plotted. We also plot the—roughly outlined—sequences

of BSGs, RSGs, and RGB/AGB stars¹⁶ of the NE part of NGC5128's halo, taken from the visual-NIR CMD of Rejkuba et al. (2001). For this, we project the stars of UKS 2323-326 to the distance of NGC5128, by adding the difference of the distance moduli of the two galaxies, namely $\delta\mu = 1.18 \pm 0.24$ ¹⁷, to all apparent stellar magnitudes of UKS 2323-326. Finally, the limiting magnitude of our K_S band is indicated by the black solid line.

Although the stellar populations of NGC5128 seem to overlap with those of UKS 2323-326 quite well, they extend towards redder $V - K_S$ values, covering a wider area on the CMD and leading to an offset between their center lines. This could be the effect of the wider range of metallicities in the stars of NGC5128 (Rejkuba et al. 2001), a view consistent with the fact that, generally, dwarf galaxies have significantly lower metallicities than giant galaxies (Mateo 1998). Moreover, this offset appears to be more dominant in the redder populations, since the BSGs of the two galaxies appear to overlap more consistently than the RSGs and the RGB/AGB stars do, implying that this offset is not a systematic error. This is an additional indication that the position of the A HST star in the YSG part of the CMD is relatively accurately determined. Other factors could also contribute to this offset, such as uncertainties in the distance moduli and/or differences in the reddening between the two fields, but these are not expected to significantly alter the global picture.

Observationally, however, our task was somewhat more difficult. On the one hand, NGC5128 is by a factor of $\sim 1.5 - 2$ more distant than UKS 2323-326, while on the other, the observations of Gullieuszik et al. (2008) were by a factor of $\sim 3 - 4$ deeper¹⁸ than our Subaru data. This is easily visible on the CMD of Fig. 6. The position of the black solid line indicates that, at best, our observations would enable us to probe only a handful of stars on the brightest tip of NGC5128's YSG/RSG branch in the much larger field studied by Rejkuba et al. (2001). The fact that we detect one of these stars is a consequence of the chosen field in a region of recent SF, which by itself increases the probability for such an observation.

Our analysis, therefore, fully supports the views of Gullieuszik et al. (2008). It suggests that it is now pos-

sible to resolve extra-galactic denser-than-average fields potentially into individual stars in galaxies located beyond our LG, using sufficiently deep AO assisted data from the current 8/10-m class telescopes. Further development of the AO systems and the upcoming class of ELT telescopes are expected to successfully undertake significantly more difficult tasks, pushing our understanding of the properties of the stellar populations of distant galaxies to a new level.

6. SUMMARY

We have performed Subaru NIR and archived HST data analysis of a field in a region of recent SF along the Cen A's jet path. The key points of our analysis are:

1. In all NIR low-pass filtered images we see strong ($> 3\sigma$ above the background mean) signal at the expected position of the brightest star in the equivalent HST field. The probability that this signal results from stochastic background fluctuations alone, at the same position, in three independent measurements is negligible ($\leq 2.5 \times 10^{-7}\%$), implying that the NIR signal originates from the NIR counterparts of this star.
2. The very good overlap of the visual and NIR colors of the brightest HST star and its absolute magnitude suggest that it is an extra-galactic YSG with an estimated age of $\sim 10^{+4}_{-3}$ Myr. The age of this star is consistent with the ages of the young blue stars that were previously identified in the region, thought to have formed after a recent jet-HI cloud interaction.
3. Based solely on their HST photometry, the second (YSG) and the third (RSG) brighter HST stars are, likely, also later-type supergiants in NGC5128 with estimated ages of $\sim 16^{+6}_{-3}$ Myr and $\sim 25^{+15}_{-9}$ Myr, respectively. The ages of the three supergiants and their indicated spread appear to be consistent with the view that the jet-HI cloud interaction was not a single episodic event, but, in fact, a continuous process during the past ~ 100 Myr. Under certain conditions, however, the third brighter HST star could also be a foreground galactic dwarf.
4. With deeper, optical/NIR, spectro-photometric observations of the entire region, using the state-of-the-art 8/10-m class telescopes equipped with AO systems, we can study a great variety of physical phenomena simultaneously and in great detail. By better determining the ages of the evolved massive stars and by accurately mapping their positions, we can constrain the most recent jet-HI

¹⁶ We choose the outline of the main distribution of the stars of Fig. 12 from Rejkuba et al. (2001) as the AGB/RGB branch of NGC5128, while we distinguish between its BSGs and RSGs by using approximate $V - K_S$ cut-offs from Table 1, namely $V - K_S < 1$ and $2.5 < V - K_S < 5.5$, respectively.

¹⁷ The adopted distance modulus of UKS 2323-326 is $\mu^{UKS2323-326} = 26.74 \pm 0.15$ mag (Gullieuszik et al. 2008).

¹⁸ In terms of integration time. This reflects a better SNR by a factor of ~ 5 with respect to our Subaru data.

cloud interaction(s) and, therefore, the underlying physics of positive AGN feedback, enrich the sample of YSGs and provide stellar parameters to the stellar evolutionary models community, and further constrain the more massive part of the IMF in this region.

ACKNOWLEDGEMENTS

We would like to thank Ass. Prof. Elias Tsakas and M.Sc. Christos Christou for the useful discussions on the mathematical rigidity of the present work. The Subaru

telescope operation team as well as the HiCIAO instrument team for their generous support. This work was supported by the Max Planck Society and the University of Cologne through the International Max Planck Research School (IMPRS) for Astronomy and Astrophysics as well as in part by the Deutsche Forschungsgemeinschaft (DFG) via grant SFB 956. We had fruitful discussions with members of the European Union funded COST Action MP0905: Black Holes in a violent Universe and the COST Action MP1104: Polarization as a tool to study the Solar System and beyond.

REFERENCES

- Bertelli, G., Nasi, E., Girardi, L., & Marigo, P. 2009, *A&A*, 508, 355
- Blanco, V. M., Graham, J. A., Lasker, B. M., & Osmer, P. S. 1975, *ApJL*, 198, L63
- Bochanski, J. J., Hawley, S. L., Covey, K. R., et al. 2010, *AJ*, 139, 2679
- Bresolin, F., Gieren, W., Kudritzki, R.-P., Pietrzyński, G., & Przybilla, N. 2002, *ApJ*, 567, 277
- Bresolin, F., Kudritzki, R.-P., Mendez, R. H., & Przybilla, N. 2001, *ApJL*, 548, L159
- Castro, N., Fossati, L., Langer, N., et al. 2014, *A&A*, 570, L13
- Castro, N., Herrero, A., Garcia, M., et al. 2008, *A&A*, 485, 41
- Charmandaris, V., Combes, F., & van der Hulst, J. M. 2000, *A&A*, 356, L1
- Deason, A. J., Belokurov, V., & Evans, N. W. 2011, *MNRAS*, 416, 2903
- Ducati, J. R., Bevilacqua, C. M., Rembold, S. B., & Ribeiro, D. 2001, *ApJ*, 558, 309
- Ekström, S., Georgy, C., Eggenberger, P., et al. 2012, *A&A*, 537, A146
- Fassett, C. I., & Graham, J. A. 2000, *ApJ*, 538, 594
- Gordon, M. S., Humphreys, R. M., & Jones, T. J. 2016, *ApJ*, 825, 50
- Graham, J. A. 1998, *ApJ*, 502, 245
- Graham, J. A., & Price, R. M. 1981, *ApJ*, 247, 813
- Gullieuszik, M., Greggio, L., Held, E. V., et al. 2008, *A&A*, 483, L5
- Hayano, Y., Takami, H., Oya, S., et al. 2010, in *Society of Photo-Optical Instrumentation Engineers (SPIE) Conference Series*, Vol. 7736, Society of Photo-Optical Instrumentation Engineers (SPIE) Conference Series
- Israel, F. P. 1998, *A&A Rv*, 8, 237
- Langer, N. 2012, *ARA&A*, 50, 107
- Malin, D. F., Quinn, P. J., & Graham, J. A. 1983, *ApJL*, 272, L5
- Mateo, M. L. 1998, *ARA&A*, 36, 435
- Morganti, R., Robinson, A., Fosbury, R. A. E., et al. 1991, *MNRAS*, 249, 91
- Mould, J. R., Ridgewell, A., Gallagher, III, J. S., et al. 2000, *ApJ*, 536, 266
- Norris, J. E. 1997, in *Astrophysics and Space Science Library*, Vol. 212, *Wide-field spectroscopy*, ed. E. Kontizas, M. Kontizas, D. H. Morgan, & G. P. Vettolani, 133
- Ohyama, Y., & Hota, A. 2013, *ApJL*, 767, L29
- Oosterloo, T. A., & Morganti, R. 2005, *A&A*, 429, 469
- Rejkuba, M. 2004, *A&A*, 413, 903
- Rejkuba, M., Greggio, L., & Zoccali, M. 2004, *A&A*, 415, 915
- Rejkuba, M., Minniti, D., Courbin, F., & Silva, D. R. 2002, *ApJ*, 564, 688
- Rejkuba, M., Minniti, D., Silva, D. R., & Bedding, T. R. 2001, *A&A*, 379, 781
- Robin, A., & Creze, M. 1986, *A&A*, 157, 71
- Robin, A. C., Haywood, M., Creze, M., Ojha, D. K., & Bienayme, O. 1996, *A&A*, 305, 125
- Salomé, Q., Salomé, P., Combes, F., & Hamer, S. 2016a, *A&A*, 595, A65
- Salomé, Q., Salomé, P., Combes, F., Hamer, S., & Heywood, I. 2016b, *A&A*, 586, A45
- Schiminovich, D., van Gorkom, J. H., van der Hulst, J. M., & Kasow, S. 1994, *ApJL*, 423, L101
- Suzuki, R., Kudo, T., Hashimoto, J., et al. 2010, in *Society of Photo-Optical Instrumentation Engineers (SPIE) Conference Series*, Vol. 7735, *Society of Photo-Optical Instrumentation Engineers (SPIE) Conference Series*
- Voigt, H.-H. 1988, *Abriß der Astronomie*.
- Zacharias, N., Finch, C. T., Girard, T. M., et al. 2013, *AJ*, 145, 44